OPEN ACCESS
JOURNAL OF ADVANCED DIELECTRICS
Vol. 11, No. 6 (2021) 2150024 (9 pages)

DOI: 10.1142/S2010135X21500247

Effect of Zr^{4+} on piezoelectric, dielectric and ferroelectric properties of barium calcium titanate lead-free ceramics

Prasanta Kumar Panda*,‡, Benudhar Sahoo*, V. Sureshkumar* and Ekaterina Dmitrievna Politova†

*Materials Science Division, CSIR-National Aerospace Laboratories
Kodihalli, Bengaluru 560017, India

†Semenov Federal Research Centre for Chemical Physics, Russian Academy of Sciences
Kosygin 4, Moscow 119991, Russia

‡pkpanda@nal.res.in

Received 10 August 2021; Revised 1 October 2021; Accepted 9 October 2021; Published 18 November 2021

$Ba_{0.85}Ca_{0.15}(Ti_{1-x}Zr_x)O_3$ (BCTZ) ceramics with x = 0.05, 0.10, 0.15, 0.20, 0.25, 0.30 were prepared by the solid-state reaction method. Calcination of the powders was carried out at 1100 °C for 4 h and the green pellets were sintered at 1400 °C for 2 h. X-ray diffraction patterns of the sintered pellets showed tetragonal splitting up to x = 0.10 while the mixture of the rhombohedral/cubic phase appeared at higher ZrO_2 concentrations. Maximum piezoelectric charge constant d_{33} = 510 pC/N and strain (S = 0.103%) were measured for BCT doped by 0.10 mol ZrO_2. Dielectric constant, remnant polarization and saturation polarization also found maxima for this composition. The Curie temperature (T_C) of the compositions decreased with increase in ZrO_2 concentration and reached 98 °C, 87 °C and 36 °C at x = 0.05, 0.10, 0.15 mol, respectively. The remaining compositions have T_C below the room temperature; therefore, they can be used for subzero/cryogenic applications. The scanning electron microscopy study revealed an increase in grain size with increase in ZrO_2 concentration and confirmed the complete solubility of ZrO_2 in the crystal lattice. Overall, low ZrO_2-doped BCT compositions with high d_{33} could be suitable for low temperature (< 80 °C) applications.

Keywords: ZrO_2-doped BCT; lead-free piezoelectrics; high piezoelectric charge constant; Curie temperature.

1. Introduction

Research on lead-free piezoelectric materials is becoming popular because PbO present in PZT is toxic in nature and causes environmental imbalance.[1–4] Therefore, the government regulatory authorities of different countries such as the EU and the USA have imposed ban on the use of lead-based materials including PZTs.[5–7] Consequently, the researchers now shifted their research mostly towards lead-free piezoelectric materials. Low density (~ 2/3) of lead-free piezoelectric materials compared to PZT is an advantage for many applications such as hydrophone, ultrasonic sonar transducers and for aerospace applications.[8,9] A number of lead-free piezoelectric ceramics such as Bismuth–Sodium Titanate (BNT), Bismuth–Potassium Titanate (BKT) and Potassium–Sodium Niobate (KNN) have been developed in the last two decades.[10–14] However, these materials have many disadvantages such as: (i) volatilization of sodium and potassium during calcinations and sintering stages produces a nonstoichiometric composition, (ii) highly corrosive at higher processing temperature which degrades the inner lining of the furnace, (iii) low piezoelectric constant (d_{33}) and (iv) high conductivity which leads to current leakage; therefore, it is difficult to do poling.[15,16] Owing to the above difficulties of alkali-based systems, barium titanate ($BaTiO_3$) modified lead-free piezoelectric systems are preferred due to advantages such as: (i) absence of volatile components, (ii) broad sintering temperature range and (iii) produces very high piezoelectric coefficient (d_{33}).[17–19] Liu *et al*.[18] first reported that the BCT–BZT composition exhibited an exceptional piezoelectric property (d_{33} ~ 620 pC/N) comparable to lead zirconate titanate (PZT) near a tri-critical point (TCP) in the phase diagram. Rherig *et al*.[20] reported a piezoelectric charge constant (d_{33}) of 355 pC/N for 0.045 and 0.085 mol Zr^{4+}-doped $BaTiO_3$ prepared by the templated grain growth method. Yu *et al*.[21] in their study mentioned d_{33} of ~236 pC/N for 0.05 mol ZrO_2-doped $BaTiO_3$. Dong *et al*.[22] prepared 0.06 mol ZrO_2-doped $BaTiO_3$ by sintering the pellets at 1400°C for 100 h and reported high d_{33} of 420 pC/N. Li *et al*.[23] studied the effect of CaO on the properties of $(Ba_{1-x}Ca_x)(Ti_{0.95}Zr_{0.05})O_3$ ceramics. A maximum piezoelectric charge constant (d_{33}) of 365 pC/N was reported by the authors for 0.08 mol of CaO-doped BCTZ with shifting of orthorhombic-tetragonal phase transition toward room temperature. The authors also prepared BCTZ ceramics by simultaneous addition of CaO and ZrO_2 (discretely) and reported d_{33} in between 325–387pC/N.[24,25] Similarly, a number of researchers also tried co-doping of Ca^{2+} and Zr^{4+} in a discrete manner and studied the properties

‡Corresponding author.

of $(Ba_{1-x}Ca_x)$-$(Ti_{1-y}Zr_y)O_3$ ceramics.[26–30] There is not much systematic study on the effect of change in ZrO_2 concentration on the properties of the $(Ba_{0.85}Ca_{0.15})(Ti_{1-x}Zr_x)O_3$ system except a few. Wu *et al*.[31] studied the effect of Zr^{4+} by varying its concentration (0–20%) and reported a maximum d_{33} of 423 pC/N at $x = 10\%$ with an optimizing poling condition. Sahoo *et al*.[32] also studied the effect of ZrO_2 and CaO on barium titanate prepared by various processing techniques and obtained maximum d_{33} of 215, 350 and 200 pC/N for a sample processed by combustion synthesis, planetary milling and microwave sintering, respectively. In this paper, an effort has been made to study the effect of zirconia concentration on piezoelectric, dielectric and ferroelectric properties of the $Ba_{0.85}Ca_{0.15}(Ti_{1-x}Zr_x)O_3$ (BCTZ) system.

2. Experimental

Basic raw chemicals such as barium carbonate (99%, Loba Chemie), calcium carbonate (> 99% Sigma-Aldrich), titanium dioxide (> 99% Sigma-Aldrich) and zirconium dioxide (99%, Sigma-Aldrich) were used for the synthesis of the compositions. Chemicals were weighed accurately as per the stoichiometric calculation and mixed thoroughly using ethyl alcohol in a roller mill for 24 h. The powder slurry was removed from the container, dried and calcined at 1100 °C for 4 h. The powders were again milled to reduce the particle size, granulated and pressed into pellets. The pellets were sintered at 1400 °C for 2 h, leveled, polished, electroded and characterized for dielectric and hysteresis measurements. For the measurement of piezoelectric charge constant, the pellets were poled at a 2.5 kV DC electric field in a silicon oil bath.

The particle size of the lead-free piezoelectric powder was measured by a particle size analyzer (Mastersizer 3000, Malvern, UK). The Scanning Electron Microscopy (SEM) analysis was carried out by an electron microscope (Model EBO 18, Zeiss, UK). Fourier Transform Infrared (FTIR) spectroscopy measurements of the calcined powder were carried out using a FTIR system (M/s. PerkinElmer, USA). X-ray diffraction patterns of the compositions were investigated by an XRD equipment (D8 Focus, Bruker) at a scanning rate of 1° per min in the 2θ range of 20–80°. Dielectric measurements were carried out using a precision impedance analyzer (6500B, Wayne Kerr Electronics, UK) with a high temperature measurement facility. Hysteresis loops and strain loops were measured with a ferroelectric loop tracer (Precision Premier II, Radian Technology, USA). The piezoelectric charge constant (d_{33}) was measured using a piezometer system (PM-35, Take Control, UK).

3. Results and Discussion

A typical particle size distribution curve of calcined and milled lead-free BCT powder doped with 0.10 mol of ZrO_2 is presented in Fig. 1.

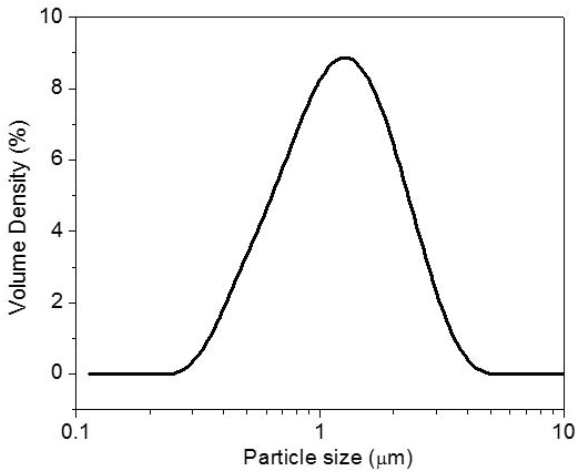

Fig. 1. Particle size curve of the 0.10 mol ZrO_2-doped BCT powder.

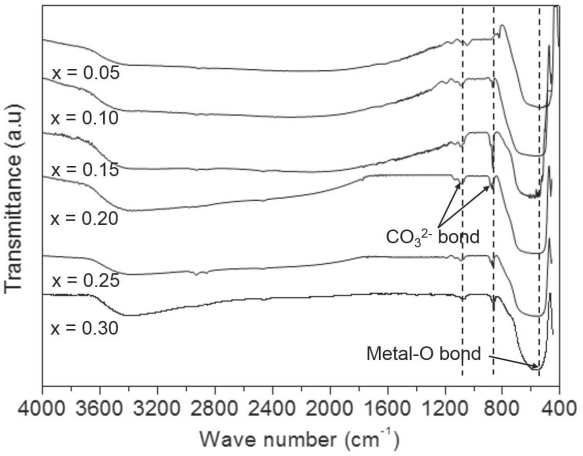

Fig. 2. FTIR spectra of different mole ZrO_2-doped BCT samples.

The graph shows a narrow sized distribution of powder particles with D_v (10), D_v (50) and D_v (90) of 0.594, 1.26 and 2.49 μm, respectively. Most of the powder particles are in the range of 0.7–1.2 μm.

Figure 2 shows the FTIR spectra of the ZrO_2-doped BCT calcined powders scanned in the wave number range of 4000–450 cm^{-1}. The spectrum displays a very broad band around 3600–3300 cm^{-1} corresponding to O–H stretching vibration. This could be due to the presence of moisture in the samples. The absorption band in the range of 550–600 cm^{-1} corresponds to Ti–O and other M–O bond vibration in the BCZT lattice. The small deep near 850 cm^{-1} and 1050 cm^{-1} could be due to C–O vibration from the residual carbonate present in the samples. Similar absorption peaks were observed by Hanani *et al*.[33] for BCTZ powders synthesized by a sol–gel hydrothermal route.

X-ray diffraction patterns of BCTZ samples with change in ZrO_2 concentration are presented in Fig. 3. All compositions showed a pure phase crystal structure which implies

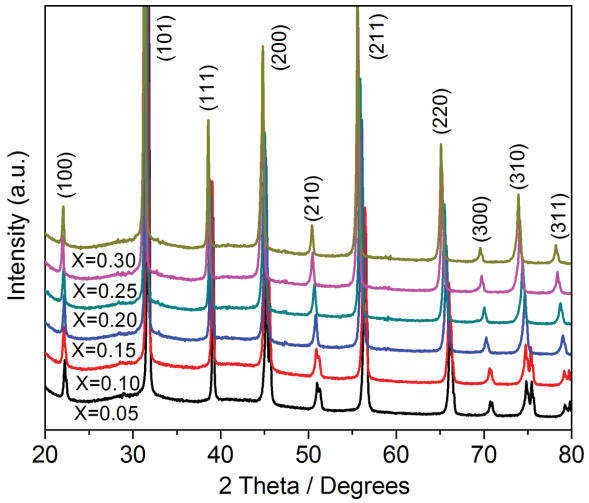

Fig. 3. XRD pattern of ZrO_2-doped BCT.

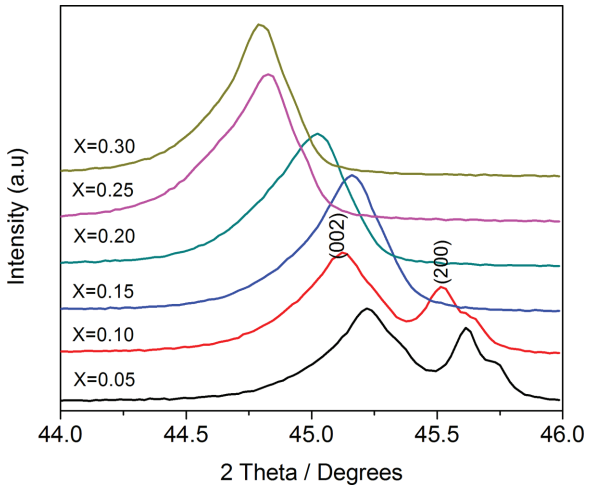

Fig. 4. Enlarged view of XRD pattern in the 2 θ range 44–46°.

that all concentrations of ZrO_2 were diffused into the crystal lattice of barium calcium titanate. Tetragonal splitting of the peaks in between 45–45.75° was observed up to the composition with $x = 0.10$ and the splitting is merged into a single peak with further increase in ZrO_2 content (Fig. 4). The coexistence of the rhombohedral and tetragonal phase could present in the composition range 0.10–0.15 mol of ZrO_2. The peak (hkl − 200) position shifted towards a lower angle with increase in ZrO_2 content. This could be attributed to the increase in the lattice parameter of the ceramics with increase in ZrO_2 concentration as the size of Zr^{4+} is larger than that of Ti^{4+}.

Scanning electron micrographs of the thermally etched BCTZ sintered pellets are shown in Fig. 5. The microstructure is found to be quite dense and uniform. The average grain size increased from 6.5 μm for the samples with 0.05 mol to 16.5 μm for samples with 0.30 mol of the ZrO_2 doped BCT. A similar increase in grain size is also observed by Wu

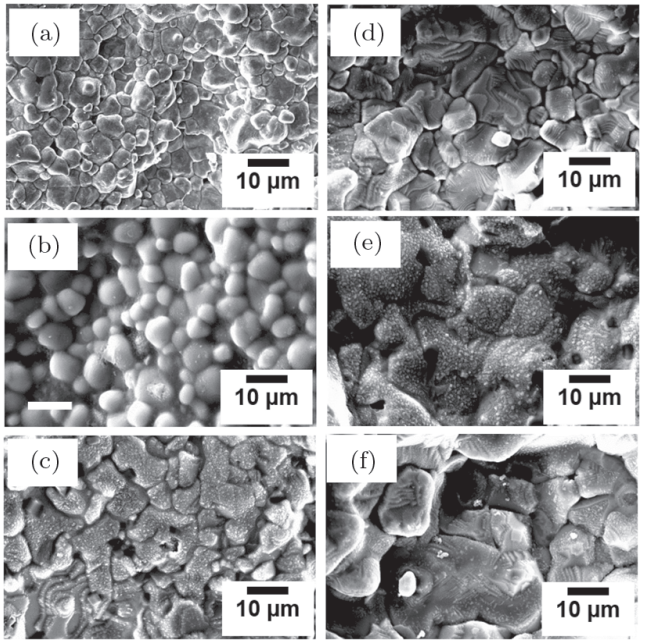

Fig. 5. SEM images of the thermally etched BCZT sintered pellets: (a) 0.05, (b) 0.10, (c) 0.15, (d) 0.20, (e) 0.25 and (f) 0.30 mol-doped ZrO_2.

et al.[31] with a larger grain of 10–25 μm for 0–20 wt.% of ZrO_2 addition. This could be due to the difference in the initial particle size of the powders and the sintering temperature used in both the studies. SEM micrographs also show that there is no segregation of ZrO_2 in the grain boundary region which is also confirmed by the EDS analysis (Fig. 6) as the weight % of the Zr element is increased on the grains. This also confirms the complete solubility of ZrO_2 in the crystal lattice which is in good agreement with the XRD analysis, as no extra peaks were observed in the XRD patterns of the samples.

Sintered densities of BCZT samples containing different amounts of ZrO_2 are presented in Table 1. It is observed that the density increased with increase in ZrO_2 concentration and maximum 95.34% is observed for 0.30 mol of ZrO_2. The increase in density could be due to complete solubility of ZrO_2 in the crystal lattice as the density of ZrO_2 (~ 5.68 g/cc) is greater that TiO_2 (4.23 g/cc). As observed from SEM, increase in grain size could also contribute for increasing the density of samples with increase in ZrO_2 concentration.

The dielectric constant of the BCTZ samples was measured with variation in the temperature and frequencies (100 Hz, 1 kHz and 10 kHz). From Fig. 7, it is clearly observed that the peak position shifted to a lower temperature with increase in ZrO_2 concentration (0.05–0.15 mol). A sharp increase in dielectric constant is observed at Curie temperature (T_C). A maximum dielectric constant of 6927 was observed for the 0.10 mol ZrO_2-doped BCTZ. T_C of the BCTZ samples decreased from 98 °C to 36 °C with increase in ZrO_2 concentration from 0.05 to 0.15 mol, respectively.

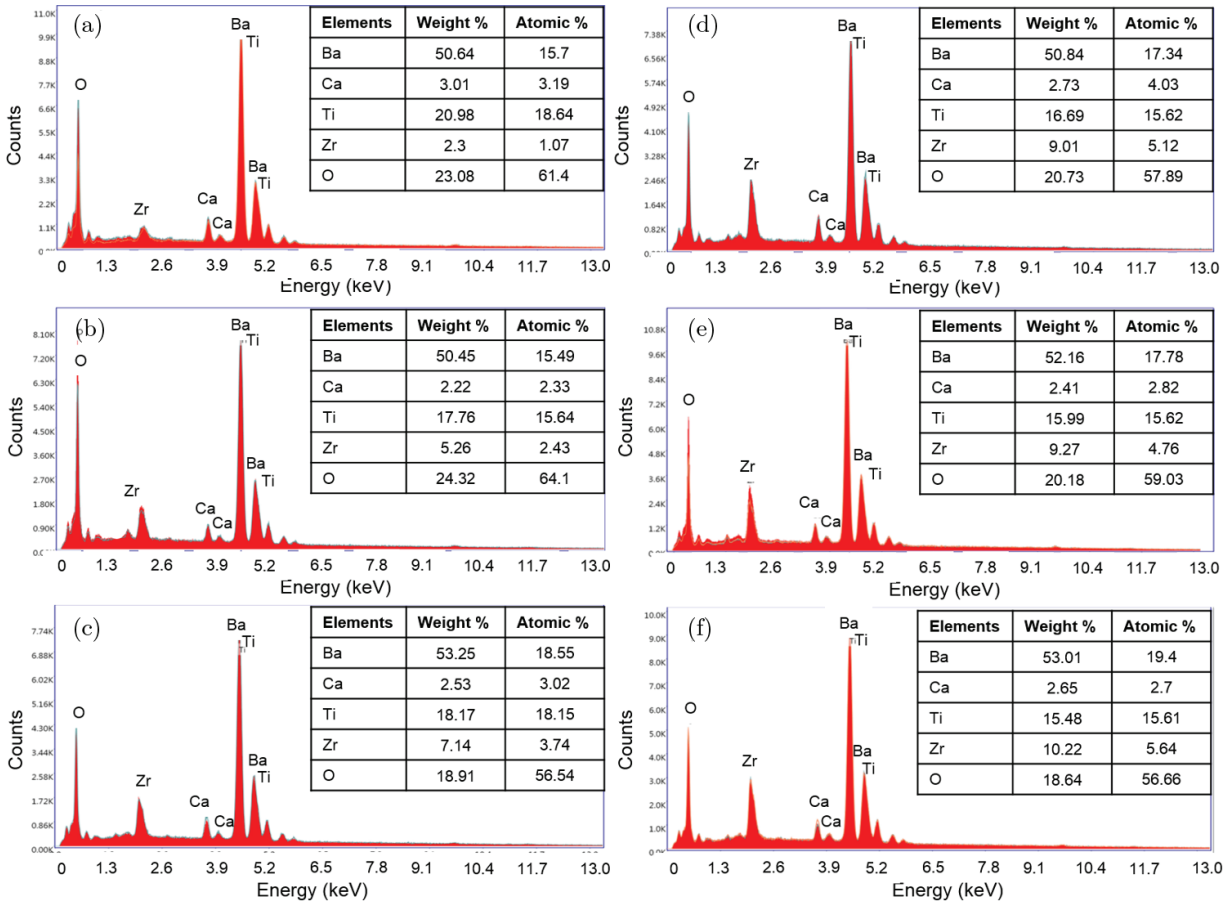

Fig. 6. EDS analysis of BCZT sintered samples: (a) 0.05, (b) 0.10, (c) 0.15, (d) 0.20, (e) 0.25 and (f) 0.30 mol-doped ZrO_2.

Table 1. Density, piezoelectric and dielectric properties of BCTZ samples sintered at 1400 °C.

Compositions	Sintered density (%)	d_{33} (pC/N)	Dielectric constant (K) at 100 Hz, RT	Loss factor (tan δ) at 100 Hz, RT	Dielectric constant (K) at T_c(100 Hz)	T_c (°C)	k_p	Q_m
$x = 0.05$	91.82	318	2390	0.0202	5049	98	0.47	74.3
$x = 0.10$	92.97	510	2534	0.0228	6927	87	0.56	94.9
$x = 0.15$	93.15	195	1981	0.0526	3448	36	0.46	50.7
$x = 0.20$	93.76	16	1563	0.0408	—	—	0.40	47.8
$x = 0.25$	94.58	5	1358	0.0119	—	—	0.36	41.3
$x = 0.30$	95.34	3	952	0.0052	—	—	0.25	21.7

The T_C further decreased below room temperature for the samples with 0.20 to 0.30 mol ZrO_2 and could not be measured due to the limitation in the measurement set up. The decrease in T_C with the addition of ZrO_2 could be due to weakening of the bond of the B-site ion and the oxygen ion in the BO6 octahedral as the size of Zr^{4+} is larger compared to that of Ti^{4+}. It also reduced the c/a ratio of the crystal lattice and allowed the phase transition from the ferroelectric phase to the paraelectric cubic phase to happen at a lower temperature, thereby decreasing the Curie temperature.[34,35]

With increase in temperature, the dielectric constant K-value increased up to T_C and then decreased. The phenomenon can be explained in terms of the alignment of dipoles as follows. The crystal structure of BCTZ is thermally excited with increase in temperature and produced a large number of unstable polarization at the ferroelectric to paraelectric phase transition temperature up to T_C. Afterwards, the dielectric constant decreased due to the increased level of thermal vibration which degrades the alignment of dipoles.[36] The loss factor (tan δ) data of the BCTZ samples were measured with variation in the temperature and frequencies and are presented

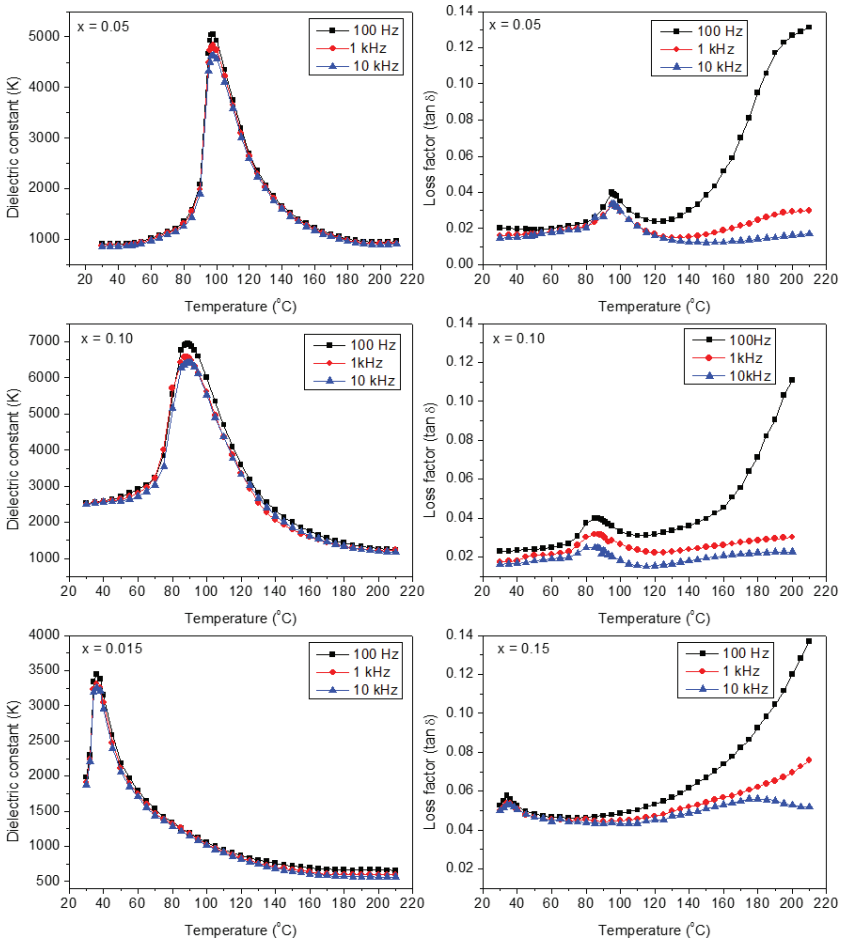

Fig. 7. Temperature dependence dielectric constant and loss factor of ZrO_2-doped BCT sample.

in Fig. 7. It is observed that the tanδ value increased with increase in temperature, a small hump was observed near the Curie temperature and the tanδ value again increased with increase in temperature.

The room temperature dielectric constant and loss factor of the sample measured at 100 Hz frequency are presented in Table 1. It is observed that the K-value increased with increase in ZrO_2 concentration, reached a maximum value of 2534 for the 0.10 mole-doped ZrO_2 and then decreased. The dielectric constant generally increased with increase in grain size.[37,38] In this study, SEM micrographs also reflect the increase in grain size, but the dielectric constant decreased after 0.10 mol of ZrO_2 which could be due to the lowering of T_c below room temperature. The loss factor of the samples increased with increase in ZrO_2 concentration up to 0.15 mol and then decreased.

The dielectric constant and loss factor of the sample with change in frequency are presented in Figs. 8 and 9, respectively. From Fig. 8, it is observed that the dielectric constant of all the compositions constantly decreased with increase in frequency up to 1 MHz. The loss factor of the samples initially decreased and then increased with increase in frequency.

The P-E hysteresis loops of the samples with ZrO_2 variation are presented in Fig. 10. It was observed that the shape of the P-E loop changes with increase in ZrO_2 content. The existence of P-E loops for the composition x = 0.05–0.15 confirms the ferroelectric behavior. The slim nature of the loop increases with increase in composition from x = 0.2 to x = 0.3 which indicates the decrease in the ferroelectric nature of the samples.[39] Remnant polarization (P_r) and coercive fields (E_c) of the samples as a function of composition are tabulated in Table 2. P_r is maximum (7.5 μC/cm^2) for the composition with x = 0.10 and then decreased with increase in ZrO_2 content. The very negligible P_r observed for the compositions with x = 0.20–0.30 could be due to their T_C falling below room temperature and also this confirms the shifting of the composition from the ferroelectric phase to a nonpolar state. The E_c of the samples decreased with increase in ZrO_2 content.

The electric field induced strain (bipolar and unipolar) of the ZrO_2-doped BZT samples is presented in Figs. 11 and 12, respectively. Typical butterfly type loops were observed for all the samples (Fig. 11). The strain as well as the area under each loop decreased with increase in ZrO_2 content.

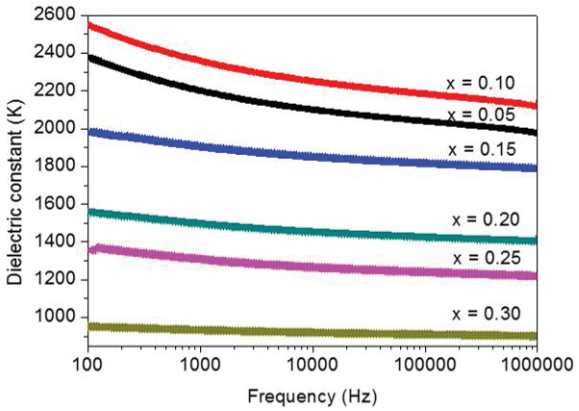

Fig. 8. Dielectric constant of ZrO_2-doped BCT sample with change in frequency.

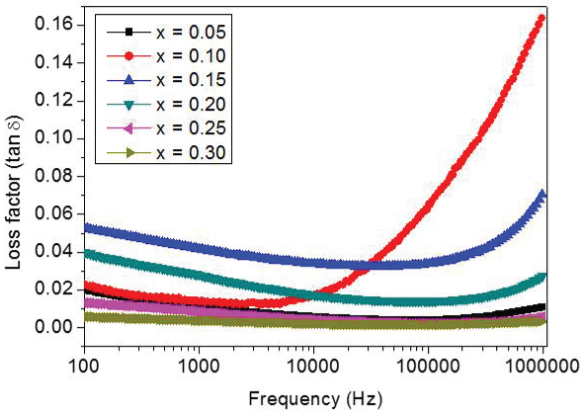

Fig. 9. Loss factor of ZrO_2-doped BCT sample with change in frequency.

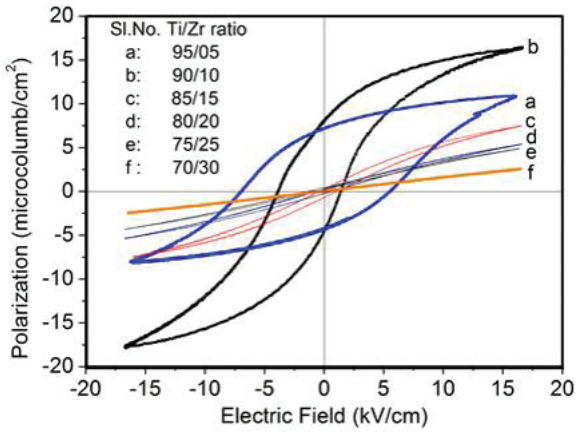

Fig. 10. Hysteresis loops of different mole ZrO_2-doped BCT samples.

Table 2. Ferroelectric properties of BCTZ samples sintered at 1400 °C.

Compositions	P_r (μC/cm^2)	E_c (kV/cm)	P_s (μC/cm^2)	E_{max} (Kv/cm)
$x = 0.05$	5.77	6.30	9.55	15.00
$x = 0.10$	7.5	2.98	17.00	16.70
$x = 0.15$	1.14	1.12	7.45	16.00
$x = 0.20$	0.75	0.83	5.52	16.55
$x = 0.25$	0.46	0.51	4.80	16.50
$x = 0.30$	0.22	0.46	2.60	16.40

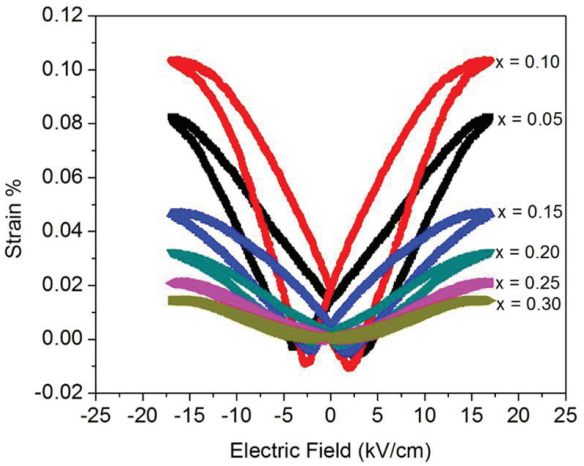

Fig. 11. Bipolar strain loops of different mole ZrO_2-doped BCT samples.

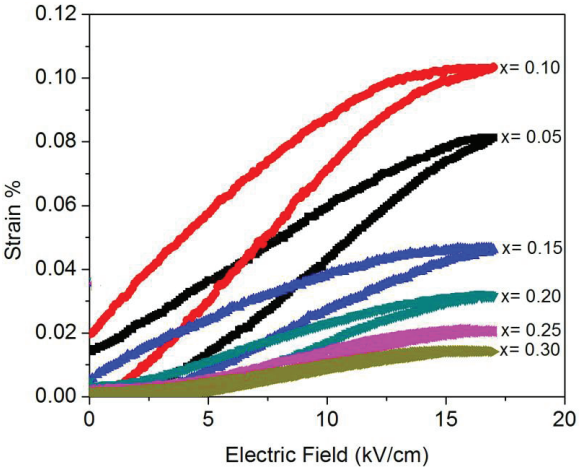

Fig. 12. Unipolar strain loops of different mole ZrO_2-doped BCT samples.

A maximum strain of 0.103% was measured for 0.10 mol. ZrO_2-doped BZT which is in consistent with d_{33} properties, i.e., large unipolar strain is associated with large piezoelectric response (Fig. 12). The compositional induced ferroelectric to nonpolar behavior with increase in ZrO_2 content was also noticed from the strain loops.[40,41] The butterfly loop with negative strain was observed for the composition x = 0.05–0.15 which is a typical ferroelectric nature of the sample.

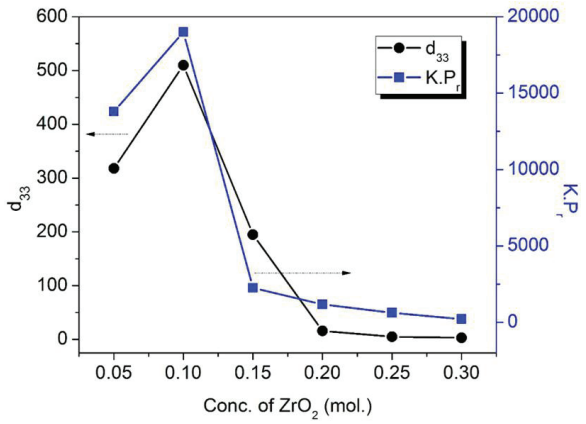

Fig. 13. Piezoelectric properties of ZrO_2-doped BCT samples.

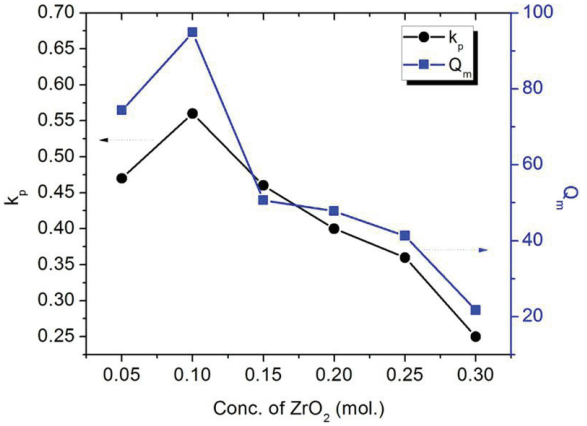

Fig. 14. k_p and Q_m of ZrO_2-doped BCT samples.

With increase in ZrO_2 content (x = 0.20–0.30) the negative strain reduced confirming the nonpolar nature of the compositions.

Piezoelectric properties of BCZT ceramics with ZrO_2 variation are presented in Fig. 13. It is observed that d_{33} increased in compositions up to 0.10 mol of ZrO_2 and thereafter it decreased. Maximum d_{33} of 510 pC/N is measured for the 0.10 mol of ZrO_2-doped BCTZ. This could be attributed to the co-existence of the rhombohedra and tetragonal phase which would enhance the dipole alignment in the applied field direction. Though the density of the samples increased with increase in ZrO_2 concentration, appreciable increase in d_{33} is not observed as the T_C of the samples falls below room temperature and also the shifting of the phase from the ferroelectric to nonpolar state was confirmed from the strain loops. The relationship between d_{33} and K.Pr is also presented in Fig. 13. It was observed that both the d_{33} and K.Pr graphs follow a similar trend, i.e., a maximum value was observed for 0.10 mol. of ZrO_2 concentration which is the MBP composition having a coexistence of the rhombohedral and tetragonal phase. The highest value of K.Pr also confirms its role on achieving the highest d_{33} at this composition.[42]

The electromechanical coupling factor (k_p) of the samples were calculated using the following equation:[43]

$$k_p = \sqrt{2.5\left(\frac{f_a^2 - f_r^2}{f_r^2}\right) + 0.038}, \quad (1)$$

where f_a and f_r are the resonance and anti-resonance frequencies, respectively. The f_a and f_r values for all the samples were measured using the precision impedance analyzer equipment (6500B, Wayne Kerr Electronics, UK). The mechanical quality factor (Q_m) of the compositions was calculated using the following equation:[44]

$$Q_m = \frac{f_a^2}{2\pi Z_m C_p f_r \left(f_a^2 - f_r^2\right)}, \quad (2)$$

where Z_m and C_p are the impedance and capacitance at fundamental resonance, respectively. The k_p and Q_m values are plotted in Fig. 14. It was observed that the k_p and Q_m values of the samples follow a trend similar to d_{33}. Maximum k_p ~ 0.56 and Q_m of 94.9 is recorded for 0.10 mol ZrO_2-doped BCT. The values were further decreased with increase in ZrO_2 content.

4. Conclusions

The effect of ZrO_2 concentration on the properties of BCTZ lead-free piezoelectric ceramics was studied. The XRD analysis showed the formation of the phase pure crystal structure which was confirmed from the SEM analysis as there were no segregations at the grain boundary region. The SEM study also revealed the increase in grain size with increase in ZrO_2 concentration. The temperature dependence of dielectric properties revealed the decrease in T_C with increase in ZrO_2 concentration. Maximum piezoelectric charge constant d_{33} = 510 pC/N, dielectric constant (K = 2534) and strain (0.103%) were measured for composition with 0.10 mol of ZrO_2 concentration at room temperature. The ferroelectric hysteresis study revealed that the remnant polarization and saturation polarization were maximum for the 0.10 molZrO_2-doped BCT. The very negligible P_r value observed for the compositions with x = 0.20–0.30 could be due to their T_C falling below room temperature and shifting of the composition from ferroelectric phase to a nonpolar state. The E_c of the samples decreased with increase in ZrO_2 content.

Acknowledgments

The authors would like to thank Dr. Anjana Jain for XRD, Mrs. Kalavati, Materials Science Division, for SEM micrographs and the Director, CSIR-National Aerospace Laboratories, Bangalore, for encouraging them to undertake this work.

References

[1]A. Y. Saito, H. Takao, T. Tani, T. Nonoyama, K. Takatori, T. Homma, T. Nagaya and M. Nakamura, Lead free piezo ceramics, *Nature* **432**, 84 (2004).

[2]J. Rodel, W. Jo, K. T. P. Seifert, E. M. Anton and T. Granzow, Perspective on the development of lead-free piezoceramics, *J. Am. Ceram. Soc*. **92**, 1153 (2009).

[3]T. Takenaka and H. Nagata, Current status and prospects of lead-free piezoelectric ceramics, *J. Euro. Ceram. Soc*. **25**, 2693 (2005).

[4]P. K. Panda, Review: Environmental friendly lead-free piezoelectric materials, *J. Mater. Sci*. **44**, 5049 (2009).

[5]A. Sepulveda, M. Schluep, F. G. Renaud, M. Streicher, R. Kuehr, C. Hagelüken and A. C. Gerecke, A review of the environmental fate and effects of hazardous substances released from electrical and electronic equipment during recycling: Examples from China and India, *Environ. Impact Assess. Rev*. **30**, 28 (2010).

[6]P. Kumari, R. Rai, S. Sharma, M. Shandilya and A. Tiwari, State-of-the-art of lead-free ferroelectrics: A critical review, *Adv. Mater. Lett*. **6**, 453 (2015).

[7]Y. Fukuda, S. Fanesan and M. Pecht, *Lead-free Legislations, Exemptions, and Compliance*, eds. S. Fanesan and M. Pecht, Chapter 2 (John Wiley & Sons, 2006), pp. 45–79.

[8]D. Lin and K. W. Kwok, Piezoelectric properties of $K_{0.47}Na_{0.47}Li_{0.06}NbO_3$–$NaSbO_3$ lead-free ceramics for ultrasonic transducer applications, *Int. J. Appl. Ceram. Technol*. **8**, 684 (2011).

[9]S. T. F. Lee, K. H. Lam, X. M. Zhang and H. L. W. Chan, High-frequency ultrasonic transducer based on lead-free BSZT piezoceramics, *Ultrasonics* **51**, 811 (2011).

[10]J. Wu, Perovskite lead-free piezoelectric ceramics, *J. Appl. Phys*. **127**, 190901(2020).

[11]E. D. Politova, N. V. Golubko, G. M. Kaleva, A. V. Mosunov, N. V. Sadovskaya, S. Yu. Stefanovich, D. A. Kiselev, A. M. Kislyuk and P. K. Panda, Processing and characterization of lead-free ceramics on the base of sodium–potassium niobate, *J. Adv. Dielectr*. **8**, 1850004 (2018).

[12]T. Badapanda, S. Venkatesan, S. Panigrahi and P. Kumar, Structure and dielectric properties of bismuth sodium titanate ceramic prepared by auto-combustion technique, *Process. Appl. Ceram*. **7**, 135 (2013).

[13]E. D. Politova, N. V. Golubko, G. M. Kaleva, A. V. Mosunov, N. V. Sadovskaya, S. Yu. Stefanovich, D. A. Kiselev, A. M. Kislyuk, M. V. Chichkov and P. K. Panda, Structure, ferroelectric and piezoelectric properties of KNN-based perovskite ceramics, *Ferroelectrics* **538**, 45 (2019).

[14]D. Wang, F. Hussain, A. Khesro, A. Feteira, Y. Tian, Q. Zhao and I. M. Reaney, Composition and temperature dependence of structure and piezoelectricity in (1-*x*) $(K_{1-y}Na_y)NbO_3$-*x*$(Bi_{1/2}Na_{1/2})ZrO_3$ lead-free ceramics, *J. Am. Ceram. Soc*. **100**, 627 (2017).

[15]C. H. Hong, H.P. Kim, B. Y. Choi, H. S. Han, J. S. Son, C. W. Ahn and W. Jo, Lead-free piezoceramics — Where to move on? *J. Materiomics*. **2**, 1 (2016).

[16]P. K. Panda and B. Sahoo, *PZT and Lead-Free Piezo Ceramics for Aerospace and Energy Applications*, eds. Y. Mahajan and R. Johnson, Handbook of Advanced Ceramics and Composites, Ch. 27 (Springer Nature Switzerland AG, 2020), pp.1081–1103.

[17]M. Acosta, N. Novak, V. Rojas, S. Patel, R. Vaish, J. Koruza, G. A. Rossetti Jr. and J. Rodel, $BaTiO_3$-based piezoelectrics: Fundamentals, current status, and perspectives, *Appl. Phys. Rev*. **4**, 041305 (2017).

[18]W. Liu and X. Ren, Large piezoelectric effect in Pb-free ceramics, *Phy. Rev. Lett*. **103**, 257602 (2009).

[19]M. Maraj, W. Wei, B. Peng and W. Sun, Dielectric and energy storage properties of $Ba_{(1-x)}Ca_xZr_yTi_{(1-y)}O_3$ (BCZT): A review, *Materials* **12**, 3641 (2019).

[20]P. W. Rehrig, S. Park, S. T. McKinstry, G. L. Messing, B. Jones and T. R. Shrout, Piezoelectric properties of zirconium-doped barium titanate single crystals grown by templated grain growth, *J. Appl. Phys*. **86**, 1657 (1999).

[21]Z. Yu, C. Ang, R. Guo and A. S. Bhalla, Piezoelectric and strain properties of $Ba(Ti_{1-x}Zr_x)O_3$ ceramics, *J. Appl. Phys*. **92**, 1489 (2002).

[22]L. Dong, D. S. Stone and R. S. Lakes, Enhanced dielectric and piezoelectric properties of $xBaZrO_3$-(1−x)$BaTiO_3$ ceramics, *J. Appl. Phys*. **111**, 084107 (2012).

[23]W. Li, Z. Xu, R. Chu, P. Fu and G. Zang, Piezoelectric and dielectric properties of $(Ba_{1-x}Ca_x)(Ti_{0.90}Zr_{0.10})O_3$ lead-free ceramics, *J. Am. Ceram. Soc*. **93**, 2942 (2010).

[24]W. Li, Z. Xu, R. Chu, P. Fu and G. Zang, High piezoelectric d_{33} coefficient of lead-free $(Ba_{0.93}Ca_{0.07})$ $(Ti_{0.95}Zr_{0.05})O_3$ ceramics sintered at optimal temperature, *Mater. Sci. Eng. B* **176**, 65 (2011).

[25]W. Li, Z. Xu, R. Chu, P. Fu and G. Zang, High piezoelectric d_{33} coefficient in $(Ba_{1-x}Ca_x)(Ti_{0.98}Zr_{0.02})O_3$ lead-free ceramics with relative high Curie temperature, *Mater. Lett*. **64**, 2325 (2010).

[26]W. Liu, L. Cheng and S. Li, Prospective of (BaCa)$(ZrTi)O_3$ lead-free piezoelectric ceramics, *Crystals* **9**, 179 (2019).

[27]M. Chandraiah and P. K. Panda, Effect of dopants (A=Mg^{2+}, Ca^{2+} and Sr^{2+}) on ferroelectric, dielectric and piezoelectric properties of $(Ba_{1-x}A_x)$ $(Ti_{0.98}Zr_{0.02})$ O_3 lead-free piezo ceramics, *Ceram. Int*. **41**, 8040 (2015).

[28]H. Bao, C. Zhou, D. Xue, J. Gao and X. Ren, A modified lead-free piezoelectric BZT–xBCT system with higher T_c, *J. Phys. D: Appl. Phys*. **43**, 465401 (2010).

[29]Y. Tian, L. Wei, X. Chao, Z. Liu and Z. Yang, Phase transition behavior and large piezoelectricity near the morphotropic phase boundary of lead-free $(Ba_{0.85}Ca_{0.15})(Zr_{0.1}Ti_{0.9})O_3$ ceramics, *J. Am. Ceram. Soc*. **96**, 496 (2013).

[30]M. Chandraiah, B. Sahoo and P. K. Panda, Synthesis and electrical properties of CaO doped BZT lead free piezo ceramics, *Ferroelectrics*. **494**, 192 (2016).

[31]J. Wu, D. Xiao, W. Wu, Q. Chen, J. Zhu, Z. Yang and J. Wang, Composition and poling condition-induced electrical behavior of $(Ba_{0.85}Ca_{0.15})(Ti_{1-x}Zr_x)O_3$ lead-free piezoelectric ceramics, *J. Eur. Ceram. Soc*. **32**, 891 (2012).

[32]G. K. Sahoo, Synthesis and Characterization of Zr and Ca modified $BaTiO_3$ Ferroelectric Ceramics, Ph.D. Thesis, National Institute of Technology, Rourkela, India (2015).

[33]Z. Hanani, E. H. Ablouh, M. B. Amjoud, D. Mezzane, S. Fourcade and M. Gouné, Very-low temperature synthesis of pure and crystalline lead-free $Ba_{.85}Ca_{.15}Zr_{.1}Ti_{.9}O_3$ ceramic, *Ceram. Int*. **44**, 10997 (2018).

[34]N. Binhayeeniyi, P. Sukwisute, S. Nawae and N. Muensit, Energy conversion capacity of barium zirconate titanate, *Materials* **13**, 315 (2020).

[35]S. J. Kuang, X. G. Tang, L. Y. Li, Y. P. Jiang and Q. X. Liu, Influence of Zr dopant on the dielectric properties and Curie temperatures of $Ba(Zr_xTi_{1-x})O_3$ ($0 \le x \le 0.12$) ceramics, *Scr. Mater*. **61**, 68 (2009).

[36]D. Xue, J. Gao, Y. Zhou, X. Ding, J. Sun, T. Lookman and X. Ren, Phase transitions and phase diagram of $Ba(Zr_{0.2}Ti_{0.8})O_3$-x $(Ba_{0.7}Ca_{0.3})TiO_3$Pb-free system by anelastic measurement, *J. Appl. Phys.***117**, 124107 (2015).

[37]V. R. Mudinepalli, L. Feng, W. C. Lin and B. S. Murty, Effect of grain size on dielectric and ferroelectric properties of nanostructured $Ba_{0.8}Sr_{0.2}TiO_3$ ceramics, *J. Adv. Ceram*. **4**, 46 (2015).

[38]X. G. Tang and H. L. W. Chan, Effect of grain size on the electrical properties of $(Ba,Ca)(Zr,Ti)O_3$ relaxor ferroelectric ceramics, *J. Appl. Phys*. **97**, 034109 (2005).

[39]X. Liu and X. Tan, Giant strains in non-textured $(Bi_{1/2}Na_{1/2})TiO_3$-based lead-free ceramics, *Adv. Mater*. **28**, 574 (2016).

[40]W. Bai, D. Chen, P. Zheng, J. Xi, Y. Zhou, B. Shen, J. Zhai and Z. Ji, $NaNbO_3$ templates-induced phase evolution and enhancement of electromechanical properties in <00l> grain oriented lead-free BNT-based piezoelectric materials, *J. Eur. Ceram. Soc.* **37**, 2591-(2017).

[41]W. Bai, X. Zhao, Y. Ding, L. Wang, P. Zheng, J. Hao and J. Zhai, Giant field-induced strain with low hysteresis and boosted energy storage performance under low electric field in $(Bi_{0.5}Na_{0.5})TiO_3$-based grain orientation-controlled ceramics, *Adv. Electro. Mater*. **6**, 2000332 (2020).

[42]X. Wang, J. Wu, D. Xiao, J. Zhu, X. Cheng, T. Zheng, B. Zhang, X. Lou and X. Wang, Giant piezoelectricity in potassium–sodium niobate lead-free ceramics, *J. Am. Chem. Soc*. **136**, 2905 (2014).

[43]W. P. Mason and H. Jaffe, Methods for measuring piezoelectric, elastic, and dielectric coefficients of crystals and ceramic, *Proc. IRE* **42**, 921 (1954).

[44]K. Bian, Q. Gu, K. Zhu, R. Zhu, J. Wang, J. Liu and J. Qiu, Improved sintering activity and piezoelectric properties of PZT ceramics from hydrothermally synthesized powders with Pb excess, *J. Mater. Sci. Mater. Electron*. **27**, 8573 (2016).